Immune Implication of ASF1B Gene in Hepatocellular Carcinoma

Tao Meng
The First Affiliated Hospital of Anhui Medical University
Zhong Tong
The Third Affiliated Hospital of Anhui Medical University
Ming-Ya Yang
The First Affiliated Hospital of Anhui Medical University
Jing-Jing Wang
The First Affiliated Hospital of Anhui Medical University
Li-Xin Zhu (zhulixin@ahmu.edu.cn)
The First Affiliated Hospital of Anhui Medical University
Yan Zhang
The First Affiliated Hospital of Anhui Medical University
Yu Liu
The First Affiliated Hospital of Anhui Medical University
Zhen-Zhen Wang
The First Affiliated Hospital of Anhui Medical University

Research Article

Keywords: ASF1B, immune cells, HCC, prognosis, nomogram

Posted Date: April 30th, 2021

DOI: https://doi.org/10.21203/rs.3.rs-455248/v1

Immune Implication of ASF1B Gene in Hepatocellular Carcinoma

Tao Meng[1†], Zhong Tong[2†], Ming-Ya Yang[1], Jing-Jing Wang[1], Yan Zhang[1], Yu Liu[1], Zhen-Zhen Wang[1], Li-Xin Zhu[1*]

[1]Department of General Surgery and Centre Laboratory, The First Affiliated Hospital of Anhui Medical University, Hefei, China

[2]Department of General Surgery, The Third Affiliated Hospital of Anhui Medical University, Hefei, China

† These authors have contributed equally to this work and share first authorship

*** Correspondence:**

Li-Xin Zhu

zhulixin@ahmu.edu.cn

Keywords: ASF1B, immune cells, HCC, prognosis, nomogram

Abstract

Background: Anti-silencing function 1B (ASF1B) has been demonstrated to contribute to tumorigenesis. However, its carcinogenic and immune effects in hepatocellular carcinoma (HCC) have not been reported. This study aimed to identify immune role of ASF1B in HCC.

Methods: HCC datasets obtained from The Cancer Genome Atlas (TCGA) database were used to investigate the role of ASF1B gene in HCC, followed by validation using Gene Expression Omnibus (GEO) datasets and Gene Expression Profiling Interactive Analysis (GEPIA) website. CIBERSORT analysis was performed to evaluate immune cell infiltration levels. The TISIDB and cBioPortal network tool were used to seek ASF1B-associated immunomodulators and its co-expressed genes. TCGA cohort was divided into train set and test set according to the ratio of 7:3. Cox regression was used to identify ASF1B-associated prognostic immunomodulators in train set, followed by internal validation using the test set. Based on the median risk-score, HCC patients were divided into high- and low-risk group for the further survival curves and receiver operating characteristic (ROC) analysis, as well as nomogram and calibration curves analysis. Finally, the dataset collected from the GEO was adopted for external validation.

Results: ASF1B was over-expressed in TCGA HCC cohort and contributed poor prognosis, which was verified in two GEO datasets (GSE14520 and GSE6764) and GEPIA, as well as Kaplan Meier Plotter network tool. The immune cell infiltration levels were found to be associated with the ASF1B copy numbers and mRNA expression. A total of 78 ASF1B-associated genes were screened out, including 7 immunoinhibitors, 21 immunostimulators and 50 tightly co-expressed genes. Finally, 5 ASF1B-associated genes (TNFSF4, TNFRSF4, KDR, MICB and CST7) were identified to be strongly related to HCC survival. Survival analysis demonstrated that the prognosis of patients in high-risk group was poor. The prognosis predict model, which was established by nomogram based on risk-score, and was validated in both TCGA test set and GEO validated datasets, exerted excellent predictive power in this

study.

Conclusion: Our findings showed that the ASF1B was associated with HCC immunity. The selected ASF1B-asociated immune markers could be promising biomarkers for the prognosis of HCC.

Keywords: ASF1B, immune cells, HCC, prognosis, nomogram

Introduction

Liver cancer is the sixth most common tumor and the fourth most common cause of cancer-related death worldwide (1). An increased risk of HCC is associated with the fundamental chronic liver disease such as hepatitis B and C virus infection (2, 3). Hepatocellular carcinoma (HCC) constitutes 75%-85% of primary liver cancers with an unclear mechanism and poor prognosis (4, 5). Although immunotherapy has become a promising alternative therapy for patients with HCC (6, 7), just a proportion of HCC patients benefit from immunotherapy (8), which may result from the limited effective target. Prognostic immune biomarkers could help to recognize immunotherapy-responsive subgroups. Some evidence has indicated that tumor infiltrating leukocytes are related to the prognosis of cancers (9). Therefore, the molecular characteristics of the immune micro-environment within HCC need to be further explored. It is essential to fully understand HCC immunology and the molecular regulatory mechanisms to ensure the success of immunotherapy.

ASF1B is one of the histone H3-H4 chaperone anti-silencing function 1 (ASF1) paralogs (10, 11). Interestingly, studies have reported that high ASF1B expression is linked to diagnosis and prognosis of breast cancer, renal cell carcinoma and cervical cancer (12-14). However, the carcinogenic effect and the immune role of ASF1B in HCC have not been reported yet.

In this study, RNA-Seq data from TCGA HCC cohort and GEO databases were analyzed to investigate the ASF1B expression in HCC and the carcinogenic effect of ASF1B. Meanwhile, ASF1B-related immunomodulators were used to analyze the associated immune pathways, and to establish clinical prognosis model.

Material and methods

Data collection

HCC datasets containing data on mRNA, gene mutation and clinical features of 374 tumors and 50 normal tissues were obtained from the TCGA project (https://portal.gdc.cancer.gov/). Three liver cancer datasets GSE6764, GSE14520 and GSE54236 were obtained from GEO (https://www.ncbi.nlm.nih.gov/geo/). To further process RNA expression data, the limma package was used for R software.

Relationship between ASF1B and clinical characteristics

The expression pattern of ASF1B was analyzed in the TCGA HCC cohort between tumor and adjacent tissues. GEPIA was used to combine GTEx data and TCGA for validation (http://gepia.cancer-pku.cn/). GSE6764 and GSE14520 were also used for verification. According to ASF1B expression, the tumor samples were divided into high and low expression groups. The survival curve of high and low groups was drawn by the Kaplan Meier method. Kaplan Meier Plotter network tool was adopted to verify the survival difference (https://kmplot.com/analysis/). Moreover, the correlation between ASF1B expression and clinical features were analyzed by logistic regression and Cox regression.

Between ASF1B and tumor mutation burden

Mutation data from TCGA LIHC was used to determine tumor mutation burden (TMB). The relationship between TMB and ASF1B expression and its impact on the overall survival (OS) were analyzed in HCC dataset.

Gene Set Enrichment Analysis

The median expression of ASF1B gene was used as the cutoff value, and all tumor samples in TCGA cohort were divided into two groups with high and low expression. Gene set enrichment analysis was used to analyze the signal pathways that were significantly related to the expression level of ASF1B. Instead of concentrating on only a handful of mostly altered genes, GSEA evaluates the genome-wide expression

profiles at the levels of gene sets. A set of genes denotes a set of concordant genes with a comparable biological function, chromosomal location, or regulation (15).

Tumor infiltrating immune cells with TCGA LIHC RNA-Seq

In order to qualify and quantify 22 types of immune cells in tissues, including seven types of T cells, naive and memory B cells, plasma cells, NK cells, and myeloid subsets, Cell type Identification by Estimating Relative Subsets of RNA Transcripts (CIBERSORT) were used (https://cibersort.stanford.edu/). The TCGA LIHC profile (fpkm format) was converted to the TPM format to make the samples more comparable (16). With CIBERSORT L22 as the reference, the TCGA LIHC mRNA expression matrix was analyzed with the CIBERSORT R script obtained from the CIBERSORT website. Empirical *P*-value was determined with Monte Carlo sampling for the deconvolution of every case (17). Samples were included in the study with $P < 0.05$.

Relationship between ASF1B and tumor immune cells infiltration

Tumor Immune Estimation Resource (TIMER) is a web server that provides a detailed study of pan-cancer tumor immune cells (cistrome.dfci.harvard.edu/TIMER/) (18). Six types of immune cells that infiltrated in HCC (B cells, $CD4^+$T cells, $CD8^+$ T cells, neutrophils, macrophage and dendritic cells) were visited via TIMER to reveal the correlations of immune cell infiltration and survival, ASF1B copy number and infiltration level.

Immunomodulators

Tumor infiltrating lymphocytes (TILs) and immunomodulators related to ASF1B were obtained from the TISIDB website to clarify the interaction of the tumor-immune system (http://cis.hku.hk/TISIDB/) (19). Immunoinhibitors and immunostimulators for gene expression that were significantly correlated with ASF1B were selected (Spearman correlation test, $P < 0.05$). Next, the ASF1B-associated immunomodulators were uploaded to cBioPortal (www.cbioportal.org). Based on RNA-seq data from cancer samples, the queried genes were able to seize 50 simultaneously altered genes. The obtained proteins were used to analyze protein interaction by STRING network

tool (https://string-db.org/), and performed GO and KEGG analysis (http://consensuspathdb.org/).

Survival analysis

The TCGA cohort was separated into train set and test set with the ratio of 7:3. Univariate and multivariate COX regression were used in train set to analyze ASF1B-related immune genes to screen out prognostic-related immune genes. Risk-score was generated based on coefficient: risk-score = $\beta_1 x_1 + \beta_2 x_2 + ... + \beta_i x_i$. X_i was the expression level of each gene, and β_i was the coefficient of each gene obtained from the Cox model. Kaplan Meier curve was used to assess the risk-score of immune-related gene with OS. The time-dependent receiver operating characteristic (ROC) curves were adopted to determine the prognostic accuracy of the risk-score.

Construction of nomogram

In cancer prognosis, nomogram is widely used to estimate of the probability of a single event, such as death or recurrence, tailored to a single patient's characteristics. In this study, patients' parameters and risk-scores were integrated to form the nomogram to analyze the prognosis. The nomogram was created by the rms package of R software. To measure the predictive precision of the nomogram, the concordance index (C-index) and calibration plot were used. Calibration curves were used with the application of the bootstrap method (1,000 replicates) to visualize the deviation of predicted probabilities from what actually happened.

Internal validation and external validation

The TCGA test set and GSE54236 were used for internal validation and external validation, respectively. The risk-score of each HCC patient in validated datasets was evaluated by the same formula according to the prognostic risk-score model. Then the HCC patients were divided into two groups based on the median risk-score. The survival curves, ROC curves as well as calibrations were applied to assess the predicted power of the model.

Statistics

All statistical analysis processes were carried out with R software (version 4.0.3). GSEA software was used for GSEA set enrichment analysis (GSEA Desktop Application v4.1, Broad Institute, Inc, Cambridge, MA, USA). Wilcoxon rank sum test was used to analyze the differential expression of ASF1B, univariate and multivariate COX regression analysis were used to analyze prognosis-related genes. $P < 0.05$ was considered to be statistically significant.

Results

ASF1B was over-expressed in HCC and predicted poor prognosis

For the first time, we found that ASF1B expression in tumors was significantly higher than that of adjacent tissues based on differential expression between 374 cases of HCC tissues and 50 cases of adjacent tissues in TCGA RNA-Seq dataset (**Figure 1a-b**), similar results can also be found in two GEO datasets (GSE6764 and GSE14520) (**Figure 1c-d**) as well as the GEPIA (**Figure 1e**). Correlation analysis shown that ASF1B expression was associated with age, gender, AJCC stage, grade and T classification in TCGA datasets (**Figure 2**). The prognosis for high ASF1B expression was worse than low expression group in TCGA datasets (**Figure 3a**) and Kaplan Meier Plotter (**Figure 3b**). Logistic regression and COX regression also showed ASF1B was the independent risk factor in HCC (**Table 1-2**).

Relationship between ASF1B and tumor mutation burden

We also studied the LIHC mutation data from TCGA, which was divided into two groups with high and low mutations according to the TMB score. The results showed that the survival of patients in the low TMB group was better than that in the high group (**Figure 4a**). Next, we compared the mutations status in the high and low ASF1B expression groups and found that TMB was significantly associated with ASF1B expression. High expression of ASF1B was associated with high mutation of some genes, with the highest mutation in TP53 (**Figure 4b-d**). These results suggested a possibility that ASF1B mediated mutation that might involve in the occurrence and

development of HCC.

Gene Set Enrichment Analysis

To explore the up-regulated ASF1B expression associated pathways in HCC, GSEA analysis was used to study the datasets of tumor samples collected from TCGA. We found that elevated ASF1B participated in several paths, such as cell cycle, p53 signaling pathway, mTOR signaling, Fc gamma receptor-mediated phagocytosis, T cell receptor and natural killer cell mediated cytotoxicity, that were involved in cell proliferation and immunity (**Figure 5**).

Infiltration of immune cells in HCC and normal tissues

The CIBERSORT method was used to extract and process the TCGA RNA-Seq profile, and the pattern of immune cells was systematically described. By including samples with $P < 0.05$, an overview of the immune cell infiltration of HCC matrix was shown in **Figure 6a**. The proportion of T cells regulatory (Tregs) and macrophages M0 were significantly increased compared to normal tissues, while B cells naive, T cells gamma delta and monocytes in HCC were reduced (**Figure 6b**). The correlation between different immune cell subgroups was shown in **Figure 6c**, indicating that there were different patterns of immune infiltration in HCC. In addition, the infiltration level of $CD8^+$ T cells and $CD4^+$ T cells as well as the expression level of ASF1B were significantly correlated with HCC survival (**Additional Figure 1**).

Relationship between ASF1B and immune cells

We discovered through TIMER that the level of immune infiltration varied with the ASF1B gene copy number in HCC, including $CD8^+$ T cells and macrophage (**Figure 7**). Moreover, some immune cell subsets in HCC that were positively or negatively correlated with ASF1B expression (**Figure 8**). Then we discussed the possible immune response signaling pathway mediated by ASF1B. Through TISIDB, 28 immunomodulators related to ASF1B were identified, including 7 immunoinhibitors (CTLA4, KDR, LAG3, LGALS9, PDCD1, PDCD1LG2 and TIGIT) and 21 immunestimulators (CD27, CD40LG, CD80, CD276, CXCL12, HHLA2, ICOS,

ICOSLG, IL6, IL6R, LTA, MICB, NT5E, TMEM173, TNFRSF4, TNFRSF9, TNFRSF18, TNFSF4, TNFSF9, TNFSF15 and ULBP1) (**Figure 9a**). Subsequently, we selected the top 50 genes strongly tied to these 28 immunomodulators by using cBioPortal for Cancer Genomics (**Figure 9b**). GO was adopted to annotate these genes and KEGG analysis suggested that these genes were involved in the processes of immune signaling (**Figure 9c-d**).

Prognostic significance of ASF1B-related immunomodulators

In order to determine the prognostic value of 78 ASF1B-related immunomodulators. We firstly identified 10 genes (KDR, PTPRCAP, TNFSF4, CD40LG, TNFRSF4, SLAMF6, MICB, TNFSF9, CD276 and LGALS9) in train set by univariate COX analysis that were significantly related to the prognosis of HCC (**Figure 10a**). Then multivariate COX analysis identified 5 genes (TNFSF4, TNFRSF4, KDR, MICB and CST7) that were the independent risk factors for the prognosis of HCC (**Figure 10b**). The risk-score was calculated by accumulating the product of these 5 genes expression and its coefficient in each sample (**Supplementary Dataset 1**). The Kaplan Meier survival curve showed that patients in the low-risk group had significantly longer OS than those in the high-risk group (**Figure 11a**). The area under the ROC curve for the 1-year, 3-year, and 5-year survival rates were 0.711, 0.723 and 0.756, respectively (**Figure 11c**). The distribution of risk-scores, survival status and characteristic gene expression profiles of HCC was shown in **Figure 12a** and **Figure 12c**. The results were verified in the test set (**Figure 11b**, **Figure 11d**, **Figure 12b, Figure 12d** and **Supplementary Dataset 2)**. Univariate COX regression analysis showed that the risk-score as well as tumor stage, T classification and Lymph node metastasis were associated with survival (**Figure 13a**), and the multivariate COX showed that the risk-score was an independent risk factor for the prognosis of HCC patients (**Figure 13b**).

Construction of nomogram

A nomogram was created to predict patient survival probability (**Figure 14a**). The curve of calibration indicated a good fit between nomogram-predicted probability and idea

reference line for the 1-year, 3-year and 5-year survival (**Figure 14b-d**). Additionally, the C-index was 0.69, which suggested a good predictive power.

Internal validation and external validation

For the purpose of examining the power of the ASF1B-asociated immune genes risk-score based model. The RNA-Seq and outcomes of TCGA test set and GSE54236 were used for internal and external validation, respectively. The risk-score of HCC patients was calculated via the same formula. The results of the test set and the train set showed a good consistency, the high-risk group suffered a higher survival risk compared with the low-risk group (**Figure 12b**). Survival curves showed that high-risk group exerted poor outcomes (**Figure 11b**), and the area under the ROC curve of 1-year, 3-year and 5-year of the predicted OS were 0.759, 0.734 and 0.713 (**Figure 11d**). In addition, similar results were observed in external validation using GSE54236 (**Supplementary Dataset 3**). The prognosis of high-risk group was poorer than low-risk group (**Figure 15a).** Due to the small sample size and short survival of this data set, we just produced the 1-year and 2-year ROC curves. The area under the ROC curves were 0.678 and 0.601 (**Figure 15b**). Furthermore, the calibration curves showed a good consistency between predicted survival and actual survival (**Figure 15c-d**).

Discussion

Many studies have identified multiple key genes related to the occurrence of liver cancer (20, 21). ASF1B have been reported as a carcinogenic gene in several cancers (12-14, 22). However, it has not been reported in HCC. From public databases analysis including TCGA and GEO datasets, it has been found that ASF1B was over-expressed in patients with HCC. The ASF1B expression was positively associated with AJCC stage, grade and T classification of patients with HCC. Consistent with our results, it has also been reported in prostate cancer that ASF1B expression is related to TNM staging and metastasis (22). Logistic and Cox regression also indicated that the higher expression of ASF1B may be an independent prognostic factor of HCC. Moreover, ASF1B was closely related to gene mutations in HCC, especially TP53 mutations. TP53

mutations were more commonly emerged in HBV-related HCC, which had a poor differentiation and prognosis (23, 24). This study presented first evidence of the link between ASF1B and prognosis as well as TMB in HCC.

Tumor micro-environment plays an important role in the pathogenesis of cancers (25, 26). In this study, the infiltration characteristics of immune cell subsets were evaluated in each patient sample. CIBERSOT analysis showed that the infiltration traits of 22 immune subgroups in HCC have changed significantly compared to normal tissues. These results showed that prognosis of HCC was closely associated with the infiltration of tumor immune cells. Therefore, molecular markers that reflect the immune status of HCC patients can be further explored.

In our study, ASF1B was found to be associated with immune cell infiltration in HCC for the first time. The copy number of the ASF1B gene was linked to the level of infiltration of $CD8^+$ T cells and macrophage in HCC. In detail, the levels of ASF1B mRNA were inversely proportional to the abundance of most immune cell types. The correlation of ASF1B and immunity was validated by GSEA of TCGA datasets.

The uniqueness of the liver is that it has an important effect on immune regulation and many metabolic functions (27). Particularly in liver cirrhosis, there is an active, immune-mediated inflammatory process (28). A KEGG pathway analysis of ASF1B-related immunomodulators in our study showed that several pathways such as PD-L1 and PD-1 checkpoint pathway in cancer, NK cell mediated cytotoxicity, NF-κB signaling pathway and T cell receptor signaling pathway could be involved in the ASF1B-mediated immune response.

In a variety of tumor types, including melanoma (29, 30), non-small cell lung cancer (31, 32), renal cell carcinoma (33) as well as liver cancer (34), immune checkpoint inhibitors such as ipilimumab (CTLA4 inhibitor) and nivolumab (PD-1 inhibitor) have proven beneficial for survival. At the late stage of HCC, the PD-1 pathway is found to inhibit T cell activation primarily within peripheral tissues (35).

For the most part, immune system process is regulated by immune cells called T cells.

T cells could identify tumor antigens in the tumor microenvironment, which are given to T cell receptors by antigen-presenting cells (APCs). There was a decrease in the number of normal T cells while an increase in damaged T cells in patients with HCC, leading to the progression of this cancer (36). Cytotoxic NK cells were activated by the multi-target kinase inhibitor sorafenib, leading to tumor cell death (37). NF-κB not only participates in fibrogenesis in chronically inflamed liver, but also participates in the initiation and promotion of HCC (38). The above results indicate that the immune-related pathways mediated by ASF1B-related immunomodulators have shown promising effects in HCC.

In considering the fact that there are few reports on the direct effect of ASF1B with the above four pathways. However, ASF1B has been reported to be involved in regulating the AKT pathway and mediating tumor proliferation (13, 22). While, the AKT pathway has reported to be involved in the regulation of PD-1, NK cells, T cells and NF-κB signaling pathway in the process of tumor immunity (39-42). Taken together with our results, although the specific mechanism of ASF1B regulating immunity has not been experimentally confirmed, ASF1B inhibitors are biologically feasible.

Finally, the immune prognosis model for HCC via ASF1B-related immunomodulators was set up in this study. From this model, risk-scores derived from gene signatures were significantly related to HCC survival. In addition, with a 0.69 C-index, a nomogram was created for personalized prediction of the prognosis. These results were verified by internal and external validation.

Conclusions

In conclusion, our results found that the over-expression of ASF1B gene might play an important role in tumor immune micro-environment control in patients with HCC, and present a poor prognosis. The predictive model obtained from ASF1B-related immunomodulators could be used to predict the OS in patients with HCC.

Acknowledgements

Not applicable.

Author contributions

TM and ZT processed the data and conducted the analyses. JW and MY prepared all the tables and figures. ZW, YL, YZ and LZ conceived and wrote the manuscript. All authors approved the final manuscript.

Funding

This research was supported by grants from the National Natural Science Foundation of China (52072005 and 51872279).

Competing interests

The authors declare no competing interests.

Data availability

Not applicable.

Ethics declarations

Not applicable.

Consent to participate

The authors confirm that informed consent was obtained to publish the information and images in an online openaccess publication.

References

1. Bray F, Ferlay J, Soerjomataram I, Siegel RL, Torre LA, Jemal A. Global cancer statistics 2018: GLOBOCAN estimates of incidence and mortality worldwide for 36 cancers in 185 countries. CA Cancer J Clin. 2018;68(6):394-424.
2. Liu Z, Jiang Y, Yuan H, Fang Q, Cai N, Suo C, et al. The trends in incidence of primary liver cancer caused by specific etiologies: Results from the Global Burden of Disease Study 2016 and implications for liver cancer prevention. J Hepatol. 2019;70(4):674-83.
3. Yang F, Ma L, Yang Y, Liu W, Zhao J, Chen X, et al. Contribution of Hepatitis B Virus Infection to the Aggressiveness of Primary Liver Cancer: A Clinical Epidemiological Study in Eastern China. Front Oncol. 2019;9:370.
4. Maucort-Boulch D, de Martel C, Franceschi S, Plummer M. Fraction and incidence of liver cancer attributable to hepatitis B and C viruses worldwide. Int J Cancer. 2018;142(12):2471-7.

5. Tabrizian P, Jibara G, Shrager B, Schwartz M, Roayaie S. Recurrence of hepatocellular cancer after resection: patterns, treatments, and prognosis. Ann Surg. 2015;261(5):947-55.
6. Zongyi Y, Xiaowu L. Immunotherapy for hepatocellular carcinoma. Cancer Lett. 2020;470:8-17.
7. Shimizu Y, Suzuki T, Yoshikawa T, Endo I, Nakatsura T. Next-Generation Cancer Immunotherapy Targeting Glypican-3. Front Oncol. 2019;9:248.
8. Inarrairaegui M, Melero I, Sangro B. Immunotherapy of Hepatocellular Carcinoma: Facts and Hopes. Clin Cancer Res. 2018;24(7):1518-24.
9. Chen B, Khodadoust MS, Liu CL, Newman AM, Alizadeh AA. Profiling Tumor Infiltrating Immune Cells with CIBERSORT. Methods Mol Biol. 2018;1711:243-59.
10. Paul PK, Rabaglia ME, Wang CY, Stapleton DS, Leng N, Kendziorski C, et al. Histone chaperone ASF1B promotes human beta-cell proliferation via recruitment of histone H3.3. Cell Cycle. 2016;15(23):3191-202.
11. Lee KY, Im JS, Shibata E, Dutta A. ASF1a Promotes Non-homologous End Joining Repair by Facilitating Phosphorylation of MDC1 by ATM at Double-Strand Breaks. Mol Cell. 2017;68(1):61-75 e5.
12. Corpet A, De Koning L, Toedling J, Savignoni A, Berger F, Lemaitre C, et al. Asf1b, the necessary Asf1 isoform for proliferation, is predictive of outcome in breast cancer. EMBO J. 2011;30(3):480-93.
13. Jiangqiao Z, Tao Q, Zhongbao C, Xiaoxiong M, Long Z, Jilin Z, et al. Anti-silencing function 1B histone chaperone promotes cell proliferation and migration via activation of the AKT pathway in clear cell renal cell carcinoma. Biochem Biophys Res Commun. 2019;511(1):165-72.
14. Liu X, Song J, Zhang Y, Wang H, Sun H, Feng X, et al. ASF1B promotes cervical cancer progression through stabilization of CDK9. Cell Death Dis. 2020;11(8):705.
15. Subramanian A, Tamayo P, Mootha VK, Mukherjee S, Ebert BL, Gillette MA, et al. Gene set enrichment analysis: a knowledge-based approach for interpreting genome-wide expression profiles. Proc Natl Acad Sci U S A. 2005;102(43):15545-50.
16. Newman AM, Liu CL, Green MR, Gentles AJ, Feng W, Xu Y, et al. Robust enumeration of cell subsets from tissue expression profiles. Nat Methods. 2015;12(5):453-7.
17. Ali HR, Chlon L, Pharoah PDP, Markowetz F, Caldas C. Patterns of Immune Infiltration in Breast Cancer and Their Clinical Implications: A Gene-Expression-Based Retrospective Study. PLoS Medicine. 2016;13(12):e1002194.
18. Li T, Fan J, Wang B, Traugh N, Chen Q, Liu JS, et al. TIMER: A Web Server for Comprehensive Analysis of Tumor-Infiltrating Immune Cells. Cancer Res. 2017;77(21):e108-e10.
19. Ru B, Wong CN, Tong Y, Zhong JY, Zhong SSW, Wu WC, et al. TISIDB: an integrated repository portal for tumor-immune system interactions. Bioinformatics. 2019;35(20):4200-2.
20. Huo J, Wu L, Zang Y. Development and Validation of a Novel Immune-Gene Pairs Prognostic Model Associated with CTNNB1 Alteration in Hepatocellular Carcinoma. Med Sci Monit. 2020;26:e925494.
21. Shibata T, Aburatani H. Exploration of liver cancer genomes. Nat Rev Gastroenterol Hepatol. 2014;11(6):340-9.
22. Han G, Zhang X, Liu P, Yu Q, Li Z, Yu Q, et al. Knockdown of anti-silencing function 1B histone chaperone induces cell apoptosis via repressing PI3K/Akt pathway in prostate cancer. Int J Oncol. 2018;53(5):2056-66.

23. Schulze K, Imbeaud S, Letouze E, Alexandrov LB, Calderaro J, Rebouissou S, et al. Exome sequencing of hepatocellular carcinomas identifies new mutational signatures and potential therapeutic targets. Nat Genet. 2015;47(5):505-11.
24. Calderaro J, Couchy G, Imbeaud S, Amaddeo G, Letouze E, Blanc JF, et al. Histological subtypes of hepatocellular carcinoma are related to gene mutations and molecular tumour classification. J Hepatol. 2017;67(4):727-38.
25. Quail DF, Joyce JA. Microenvironmental regulation of tumor progression and metastasis. Nat Med. 2013;19(11):1423-37.
26. Schulz M, Salamero-Boix A, Niesel K, Alekseeva T, Sevenich L. Microenvironmental Regulation of Tumor Progression and Therapeutic Response in Brain Metastasis. Front Immunol. 2019;10:1713.
27. Jenne CN, Kubes P. Immune surveillance by the liver. Nat Immunol. 2013;14(10):996-1006.
28. Arroyo V, Garcia-Martinez R, Salvatella X. Human serum albumin, systemic inflammation, and cirrhosis. J Hepatol. 2014;61(2):396-407.
29. Hodi FS, O'Day SJ, McDermott DF, Weber RW, Sosman JA, Haanen JB, et al. Improved survival with ipilimumab in patients with metastatic melanoma. N Engl J Med. 2010;363(8):711-23.
30. Pasquali S, Hadjinicolaou AV, Chiarion Sileni V, Rossi CR, Mocellin S. Systemic treatments for metastatic cutaneous melanoma. Cochrane Database Syst Rev. 2018;2:CD011123.
31. Borghaei H, Paz-Ares L, Horn L, Spigel DR, Steins M, Ready NE, et al. Nivolumab versus Docetaxel in Advanced Nonsquamous Non-Small-Cell Lung Cancer. N Engl J Med. 2015;373(17):1627-39.
32. Brahmer J, Reckamp KL, Baas P, Crino L, Eberhardt WE, Poddubskaya E, et al. Nivolumab versus Docetaxel in Advanced Squamous-Cell Non-Small-Cell Lung Cancer. N Engl J Med. 2015;373(2):123-35.
33. Motzer RJ, Escudier B, McDermott DF, George S, Hammers HJ, Srinivas S, et al. Nivolumab versus Everolimus in Advanced Renal-Cell Carcinoma. N Engl J Med. 2015;373(19):1803-13.
34. Xu F, Jin T, Zhu Y, Dai C. Immune checkpoint therapy in liver cancer. J Exp Clin Cancer Res. 2018;37(1):110.
35. Buchbinder EI, Desai A. CTLA-4 and PD-1 Pathways: Similarities, Differences, and Implications of Their Inhibition. American journal of clinical oncology. 2015;39(1):98-106.
36. Jia Y, Zeng Z, Li Y, Li Z, Jin L, Zhang Z, et al. Impaired function of CD4+ T follicular helper (Tfh) cells associated with hepatocellular carcinoma progression. PLoS One. 2015;10(2):e0117458.
37. Hage C, Hoves S, Strauss L, Bissinger S, Prinz Y, Poschinger T, et al. Sorafenib Induces Pyroptosis in Macrophages and Triggers Natural Killer Cell-Mediated Cytotoxicity Against Hepatocellular Carcinoma. Hepatology. 2019;70(4):1280-97.
38. Luedde T, Schwabe RF. NF-κB in the liver--linking injury, fibrosis and hepatocellular carcinoma. Nature Rev Gastroenterol Hepatol. 2011;8(2):108-18.
39. Ouyang S, Zeng Q, Tang N, Guo H, Tang R, Yin W, et al. Akt-1 and Akt-2 Differentially Regulate the Development of Experimental Autoimmune Encephalomyelitis by Controlling Proliferation of Thymus-Derived Regulatory T Cells. J Immunol. 2019;202(5):1441-52.
40. Lastwika KJ, Wilson W, 3rd, Li QK, Norris J, Xu H, Ghazarian SR, et al. Control of PD-L1 Expression by Oncogenic Activation of the AKT-mTOR Pathway in Non-Small Cell Lung Cancer. Cancer Res. 2016;76(2):227-38.

41. Jin F, Wu Z, Hu X, Zhang J, Gao Z, Han X, et al. The PI3K/Akt/GSK-3beta/ROS/eIF2B pathway promotes breast cancer growth and metastasis via suppression of NK cell cytotoxicity and tumor cell susceptibility. Cancer Biol Med. 2019;16(1):38-54.
42. Swathi B, Makhdum A, Elizabeth L, Fangfang Y, Krystle N, Michael W. NF- κ B signaling and its relevance to the treatment of mantle cell lymphoma. Journal of Hematology & Oncology. 2018;11(1):83.

Figure legends

Figure 1. The expression pattern of ASF1B in different datasets of HCC. (a) GSE6764. (b) GSE 14520. (c) GEPIA. (d) TCGA LIHC. (e) Paired differences in TCGA.

Figure 2. Association of ASF1B expression with clinical features. (a) Age. (b) Gender. (c) AJCC stage. (d) Grade. (e) T classification. (f) Lymphatic metastasis. (g) Distant metastasis.

Figure 3. ASF1B expression associated survival analysis. (a) TCGA. (b) Kaplan Meier Plotter.

Figure 4. Correlation between ASF1B and TMB. (a) TMB associated survival analysis. (b) Mutation pattern in high ASF1B expression group. (c) Mutation pattern in low ASF1B expression group. (d) Relationship between ASF1B and TP53 mutation.

Figure 5. Enrichment plots from gene set enrichment analysis (GSEA).

Figure 6. Immune pattern evaluated by CIBERSORT. (a) The overview of infiltrating immune cells in cancerous and normal tissues for TCGA LIHC. (b) The difference of infiltrating immune cells between tumor and normal in HCC. (c) Different correlation patterns among immune cell subsets in HCC.

Figure 7. Associations between ASF1B copy numbers in HCC.

Figure 8. Association between ASF1B expression and immune cell infiltration levels via TISIDB network tool. The black asterisks in the correlation heatmap indicated immune cell types significantly associated with ASF1B expression levels in TCGA.

Figure 9. Identification and analysis of immunomodulators associated with the ASF1B gene. (a) The heatmaps of correlation between the immunoinhibitors (left panel), immunostimulators (right panel) and the ASF1B gene in LIHC. (b) Protein–protein network of 28 ASF1B-associated immunomodulators and 50 closely related genes in LIHC, produced by the STRING online server. (c) GO annotation of 28 ASF1B-associated immunomodulators and 50 closely connected genes in LIHC. (d) KEGG pathway analysis of the above mentioned 78 genes.

Figure 10. The development of prognostic gene signatures based on 78 ASF1B-associated immunomodulators. (a) Univariate COX regression of 78 ASF1B-associated immunomodulators. (b) The hazard ratios and coefcient of ASF1B-associated prognostic genes of multivariate COX regression.

Figure 11. Establishment and internal validation of prognostic model based on risk-score of ASF1B-associated prognostic immunomodulators. (a) Survival curves of the high and low-risk group of the TCGA train set. (b) Survival curves of the high and low-risk group of the TCGA test set. (c) Time-dependent ROC curves of ASF1B-associated prognostic model of the TCGA train set. (d) Time-dependent ROC curves of ASF1B-associated prognostic model of the TCGA test set.

Figure 12. Characteristics of the ASF1B-associated prognostic signature in the TCGA dataset. The dotted line is the optimal cut-of value for dividing HCC patients into high and low-risk groups. (a) The distribution of risk-score and the survival status of HCC patients in train set. (b) The distribution of risk-score and the survival status of HCC patients in test set. (c) Heatmap of the ASF1B-associated prognostic signature expression profiles between the high and low-risk groups in train set. (d) Heatmap of the ASF1B-associated prognostic signature expression profiles between the high and low-risk groups in test set.

Figure 13. The prognostic value of the ASF1B-associated prognostic signature in the TCGA dataset. (a) Univariate COX analysis of risk-score and clinical characteristics. (b) Multivariate COX analysis of risk-score and clinical characteristics.

Figure 14. Establishment of the prognostic nomogram with the inclusion of the risk-score. (a) A nomogram for predicting 1- and 3-year survival possibilities of individual HCC patients. The calibration curve of 1-year (b), 3-year (c) and 5-year (d) survival of HCC patients . The dashed line represented a perfect uniformity between nomogram-predicted and real possibilities.

Figure 15. External validation of the ASF1B-associated prognostic risk model. (a) Kaplan-Meier survival curves of HCC patients in the high and low-risk group in GSE54236. (b) Time-dependent ROC curves analysis of the prognostic risk model based on risks core for 1- and 2-year OS probability in GSE54236. Calibration plots of 1-year (c) and 2-year (d) predicted survival.

Tables

Table 1. Logistic regression of ASF1B expression and clinical pathological characteristics

Clinical characteristics	Total (N)	Odds ratio for high FAM83D expression	95%CI	*P*-value
Stage classification (II vs I)	257	1.354	0.778 - 2.363	0.28342
(III +IV vs I)	261	1.792	1.022 - 3.172	**0.04303**
T classification (T2 vs T1)	275	1.566	0.950 - 2.593	0.07936
(T3+T4 vs T1)	274	1.911	1.154 - 3.191	**0.01235**
Gender (male vs female)	321	1.532	0.955 - 2.473	0.07835
Grade classification (G2 vs G1)	232	1.122	0.610 - 2.086	0.71344
(G3+G4 vs G1)	189	2.126	1.129 - 4.060	**0.02046**
N classification (N1 vs N0)	233	1.009	0.119 - 8.524	0.99309
Age (65 vs <65)	320	1.027	0.654 - 1.612	0.90851

CI: confidence interval. Bold values indicate $P < 0.05$.

Table 2. Univariate and multivariate analysis between ASF1B expression and overall survival among HCC patients

Parameter	Univariate analysis			Multivariate analysis		
	HR	95%CI	*P*	HR	95%CI	*P*
Age	1.006	0.989 - 1.025	0.480	1.015	0.995 - 1.036	0.149

Gender	0.778	0.487 - 1.244	0.295	1.084	0.649 - 1.808	0.759
Grade	1.013	0.743 - 1.380	0.934	1.096	0.788 - 1.524	0.587
Stage	1.879	1.466 - 2.408	**6.44E-07**	0.945	0.348 - 2.567	0.912
T	1.816	1.443 - 2.287	**3.83E-07**	1.808	0.733 - 4.459	0.199
M	3.924	1.230 - 12.519	**0.021**	1.730	0.452 - 6.623	0.424
N	2.070	0.506 - 8.471	0.312	2.395	0.407 - 14.100	0.334
ASF1B	1.072	1.035 - 1.109	**8.30E-05**	1.063	1.024 - 1.104	**0.002**

491 HR: hazard ratio. Bold values indicate $P < 0.05$.

Figures

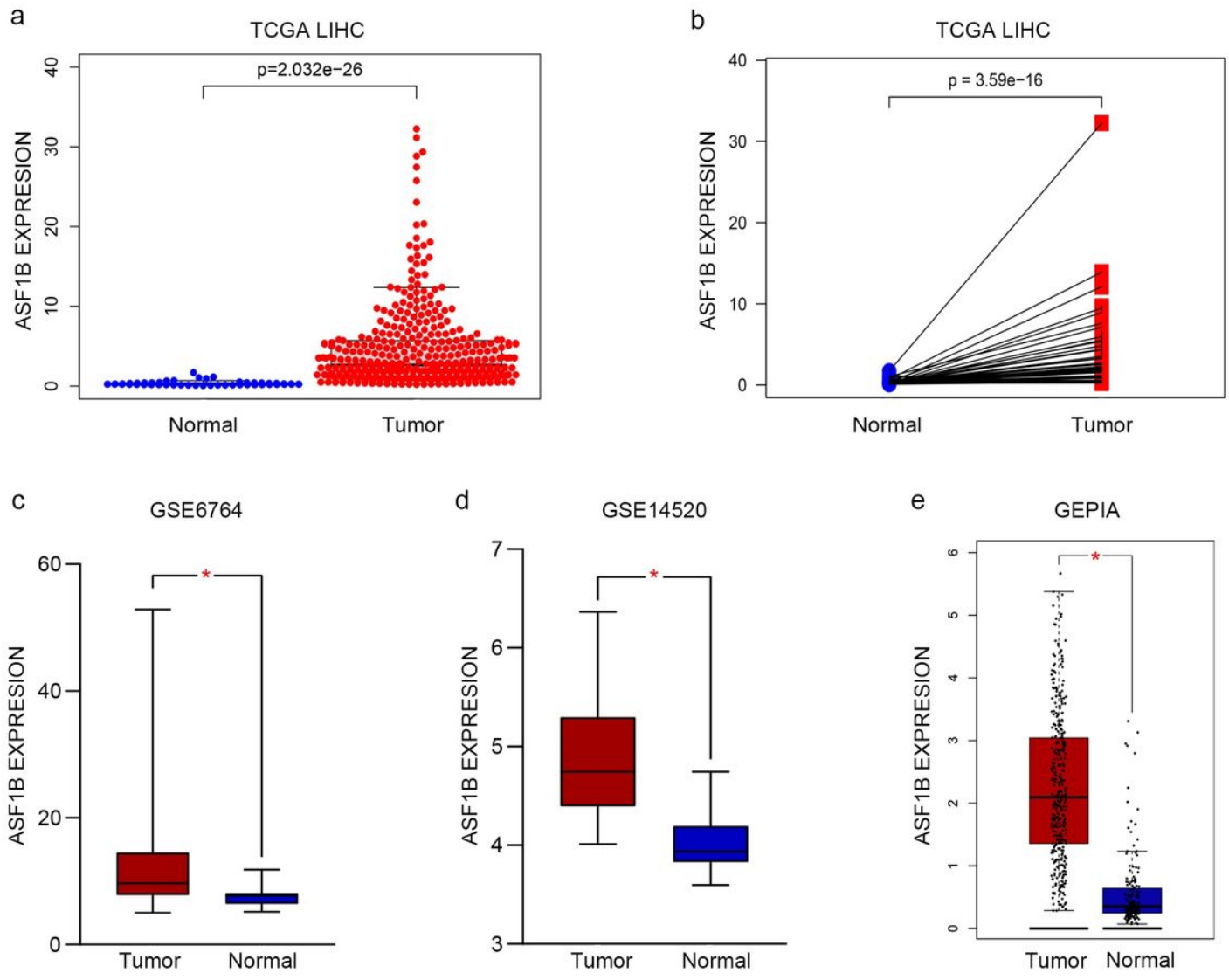

Figure 1

The expression pattern of ASF1B in different datasets of HCC. (a) GSE6764. (b) GSE 14520. (c) GEPIA. (d) TCGA LIHC. (e) Paired differences in TCGA.

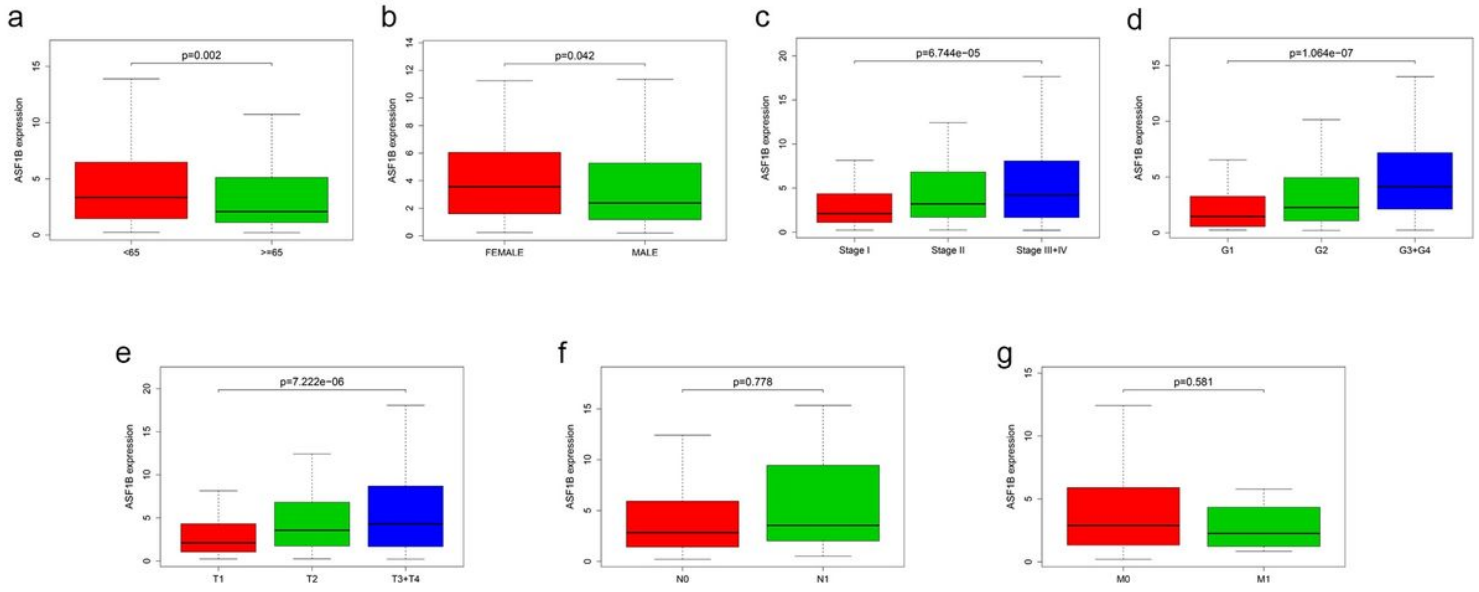

Figure 2

Association of ASF1B expression with clinical features. (a) Age. (b) Gender. (c) AJCC stage. (d) Grade. (e) T classification. (f) Lymphatic metastasis. (g) Distant metastasis.

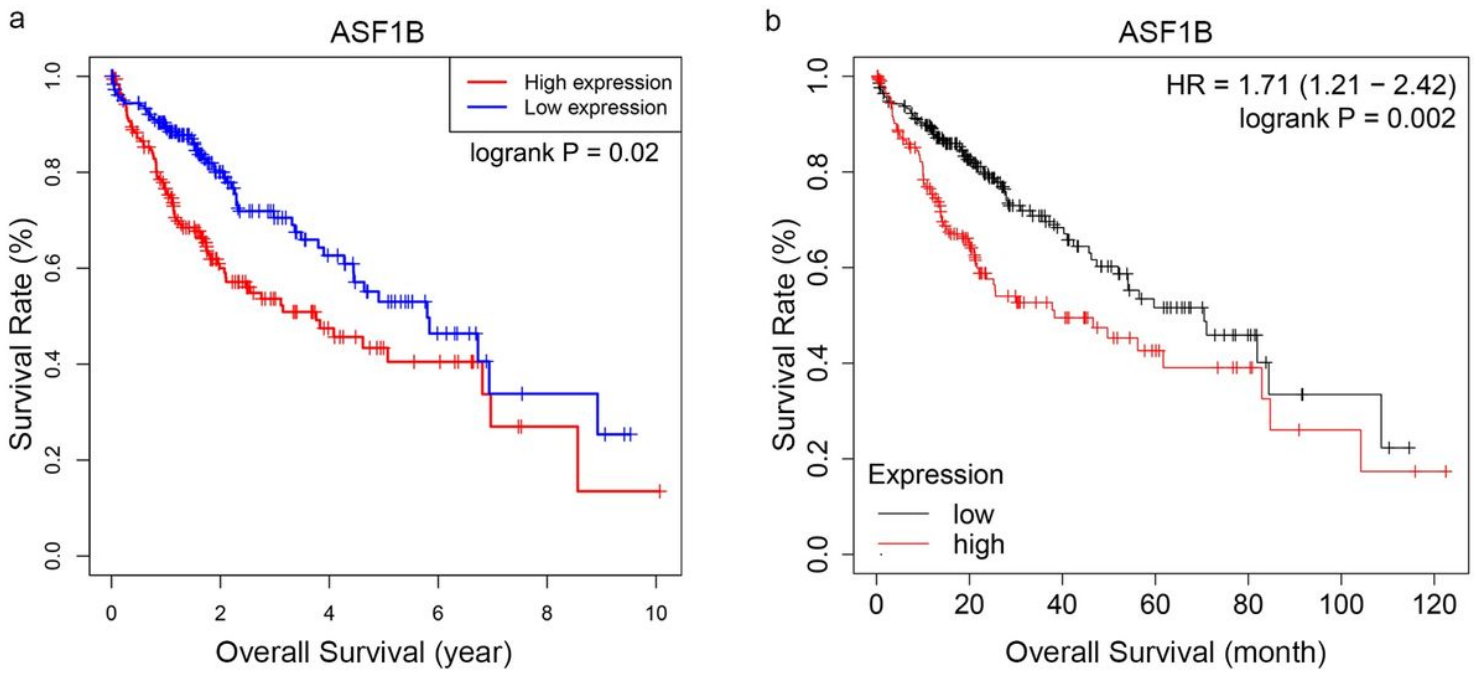

Figure 3

ASF1B expression associated survival analysis. (a) TCGA. (b) Kaplan Meier Plotter.

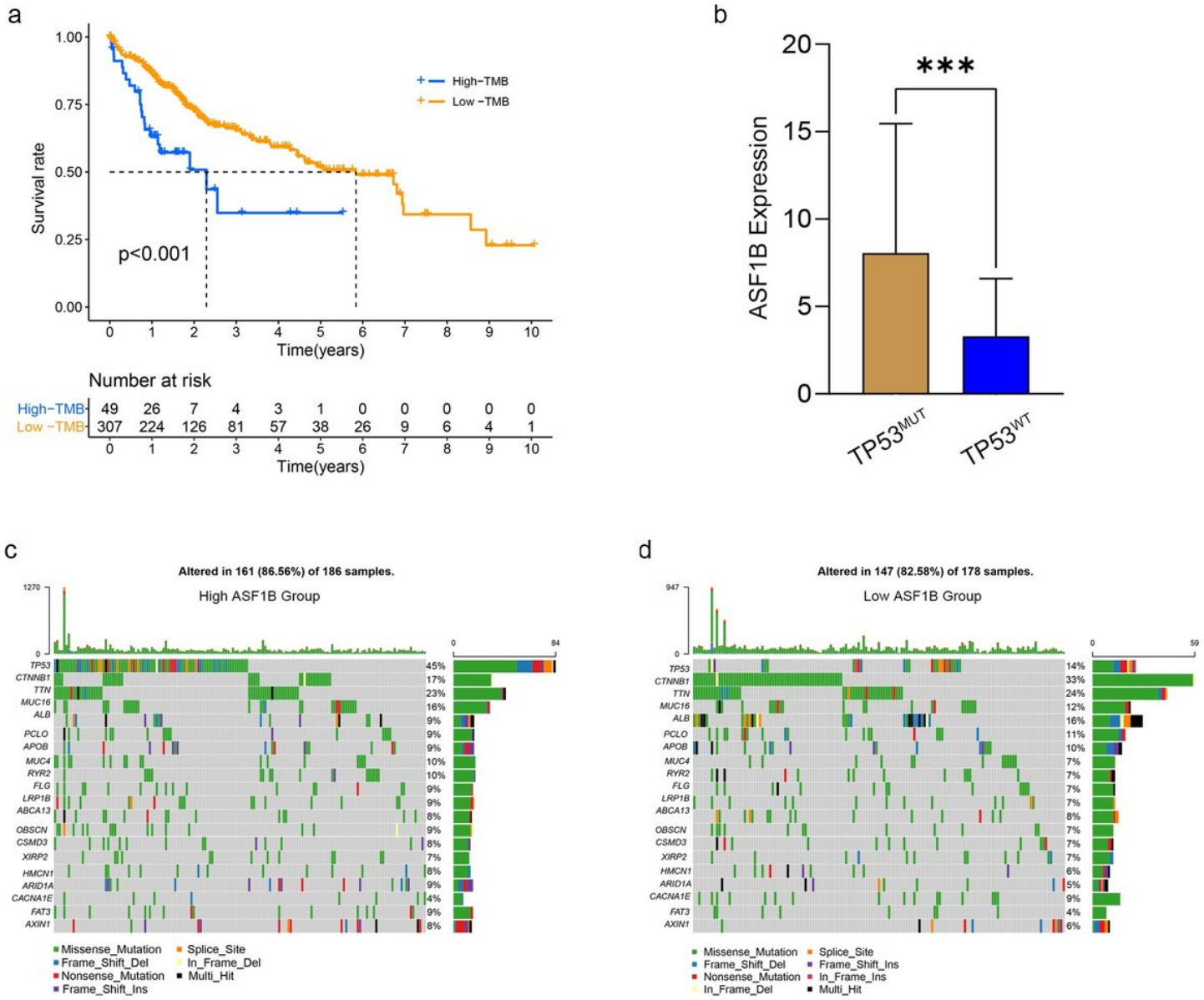

Figure 4

Correlation between ASF1B and TMB. (a) TMB associated survival analysis. (b) Mutation pattern in high ASF1B expression group. (c) Mutation pattern in low ASF1B expression group. (d) Relationship between ASF1B and TP53 mutation.

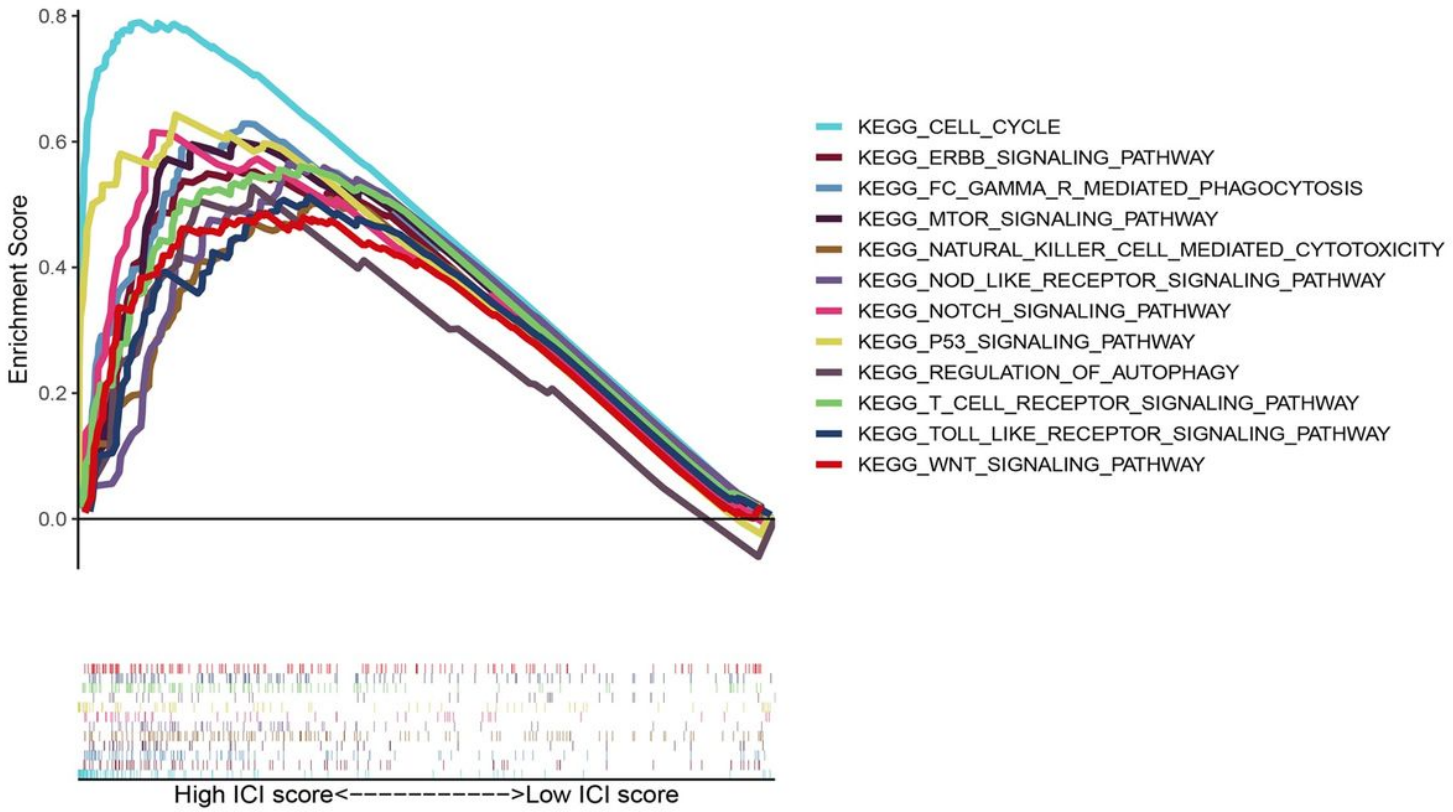

Figure 5

Enrichment plots from gene set enrichment analysis (GSEA).

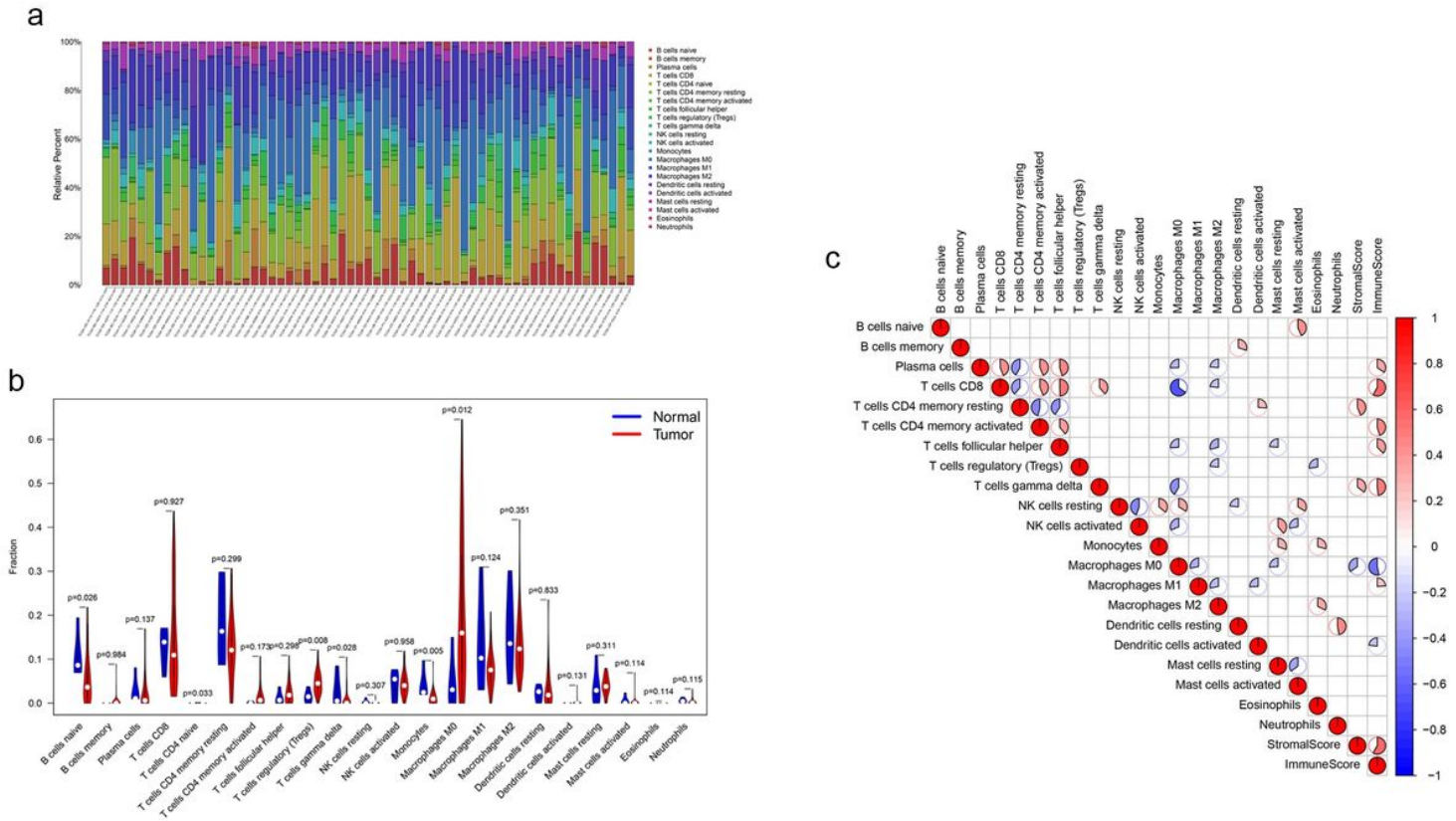

Figure 6

Immune pattern evaluated by CIBERSORT. (a) The overview of infiltrating immune cells in cancerous and normal tissues for TCGA LIHC. (b) The difference of infiltrating immune cells between tumor and normal in HCC. (c) Different correlation patterns among immune cell subsets in HCC.

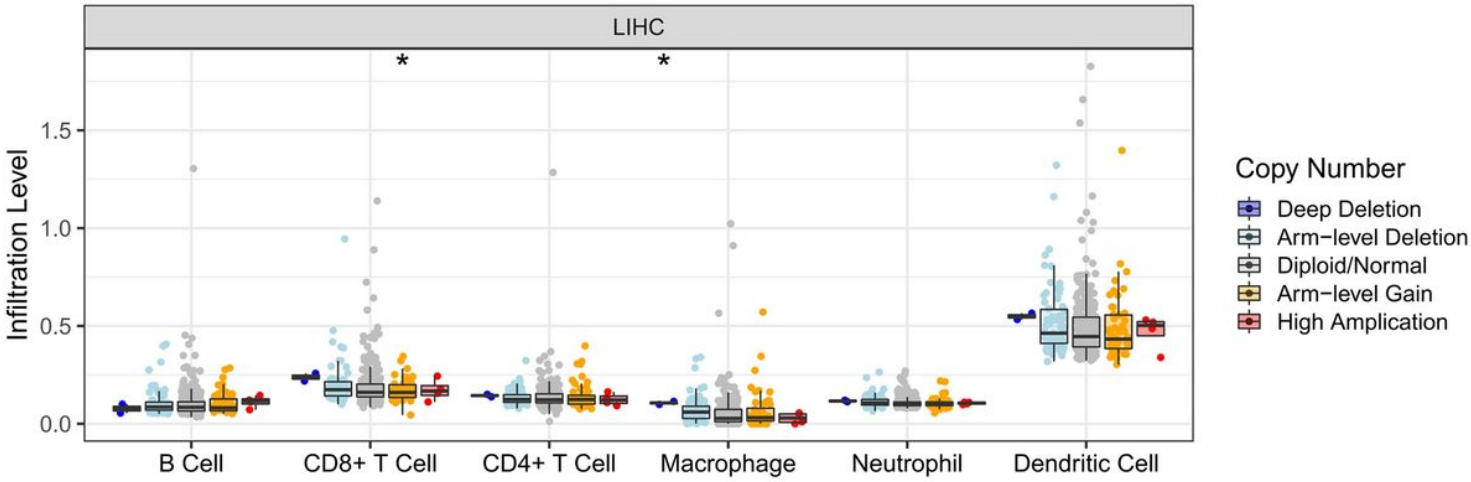

Figure 7

Associations between ASF1B copy numbers in HCC.

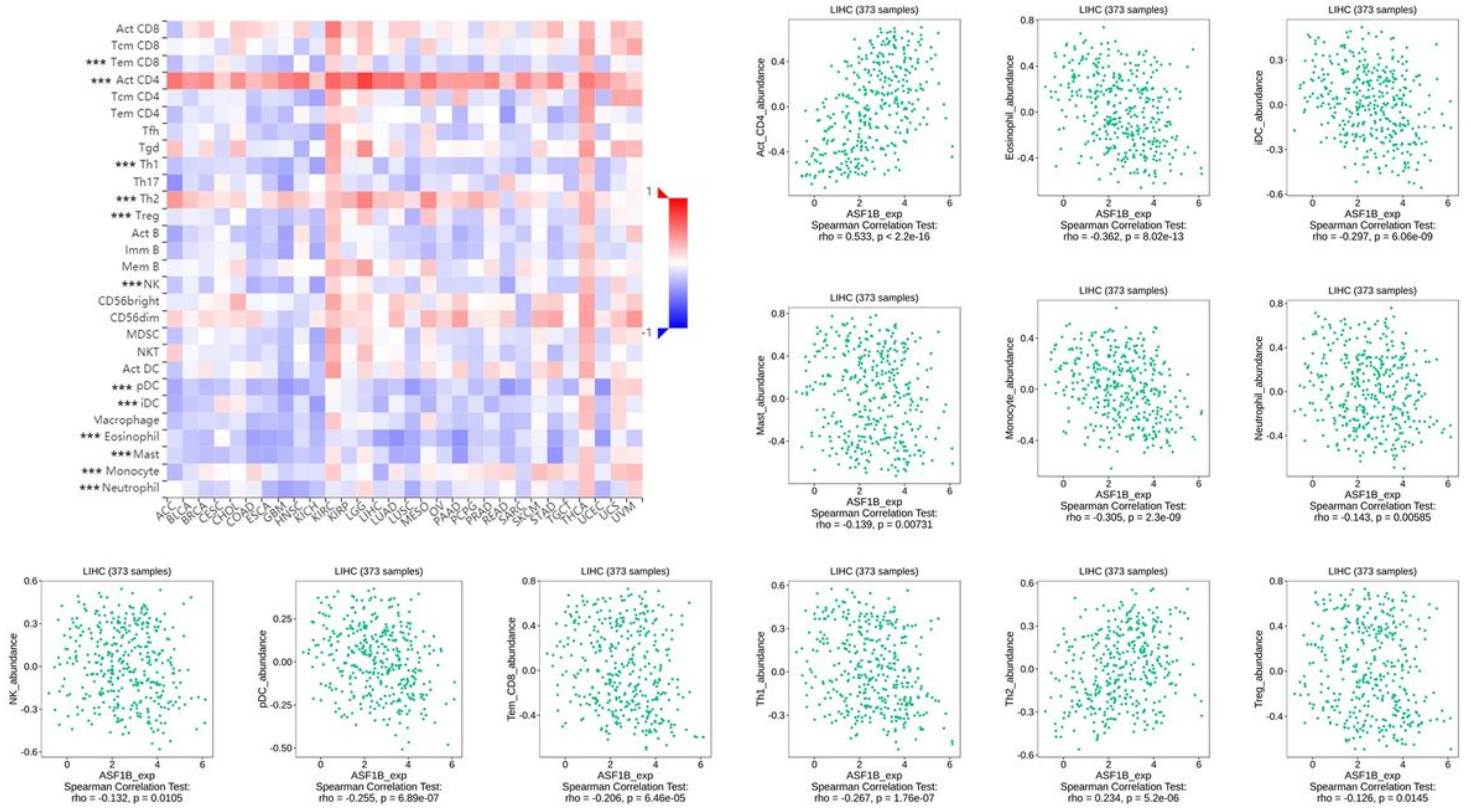

Figure 8

Association between ASF1B expression and immune cell infiltration levels via TISIDB network tool. The black asterisks in the correlation heatmap indicated immune cell types significantly associated with ASF1B expression levels in TCGA.

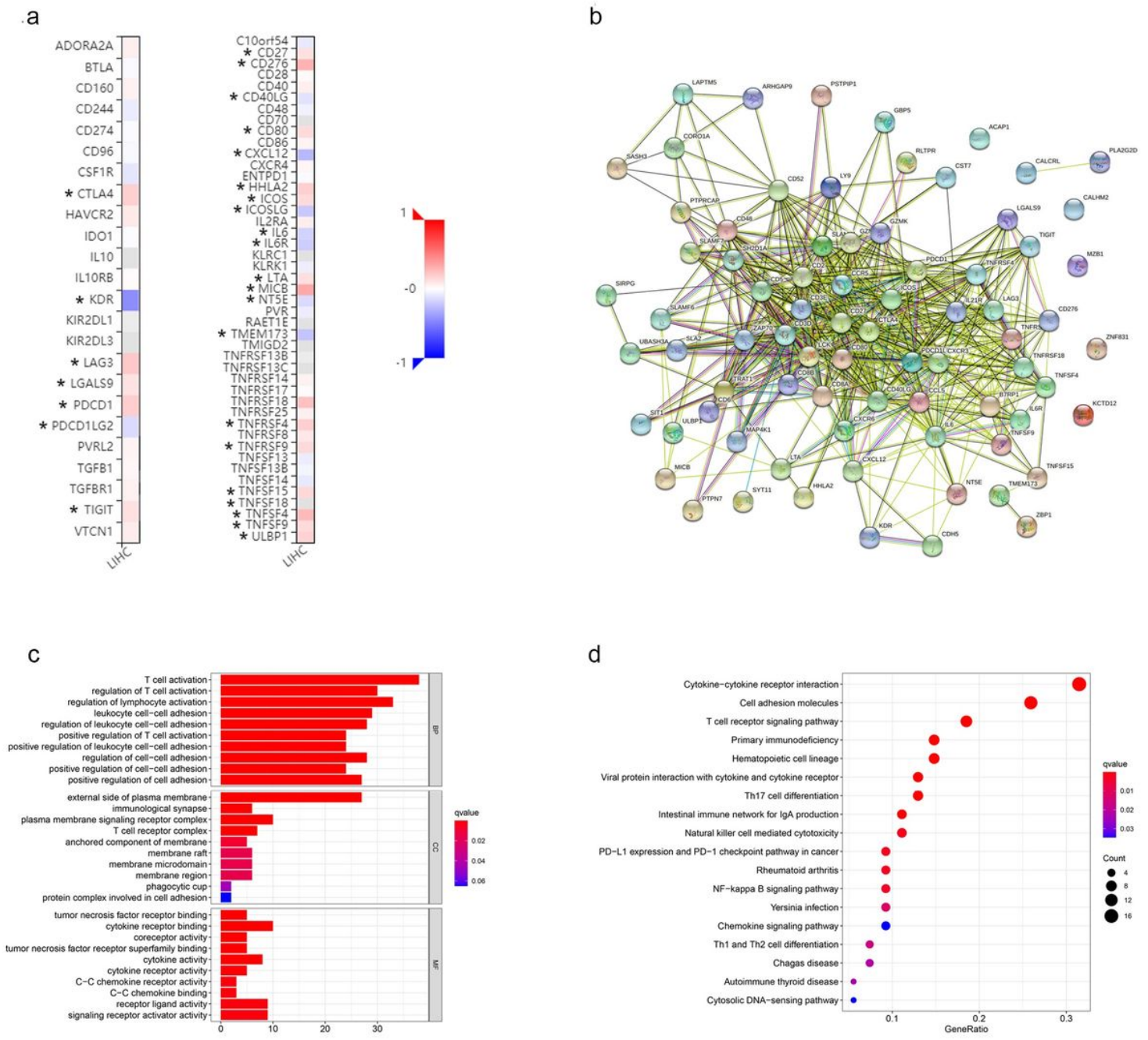

Figure 9

Identification and analysis of immunomodulators associated with the ASF1B gene. (a) The heatmaps of correlation between the immunoinhibitors (left panel), immunostimulators (right panel) and the ASF1B gene in LIHC. (b) Protein–protein network of 28 ASF1B-associated immunomodulators and 50 closely related genes in LIHC, produced by the STRING online server. (c) GO annotation of 28 ASF1B-associated immunomodulators and 50 closely connected genes in LIHC. (d) KEGG pathway analysis of the above mentioned 78 genes.

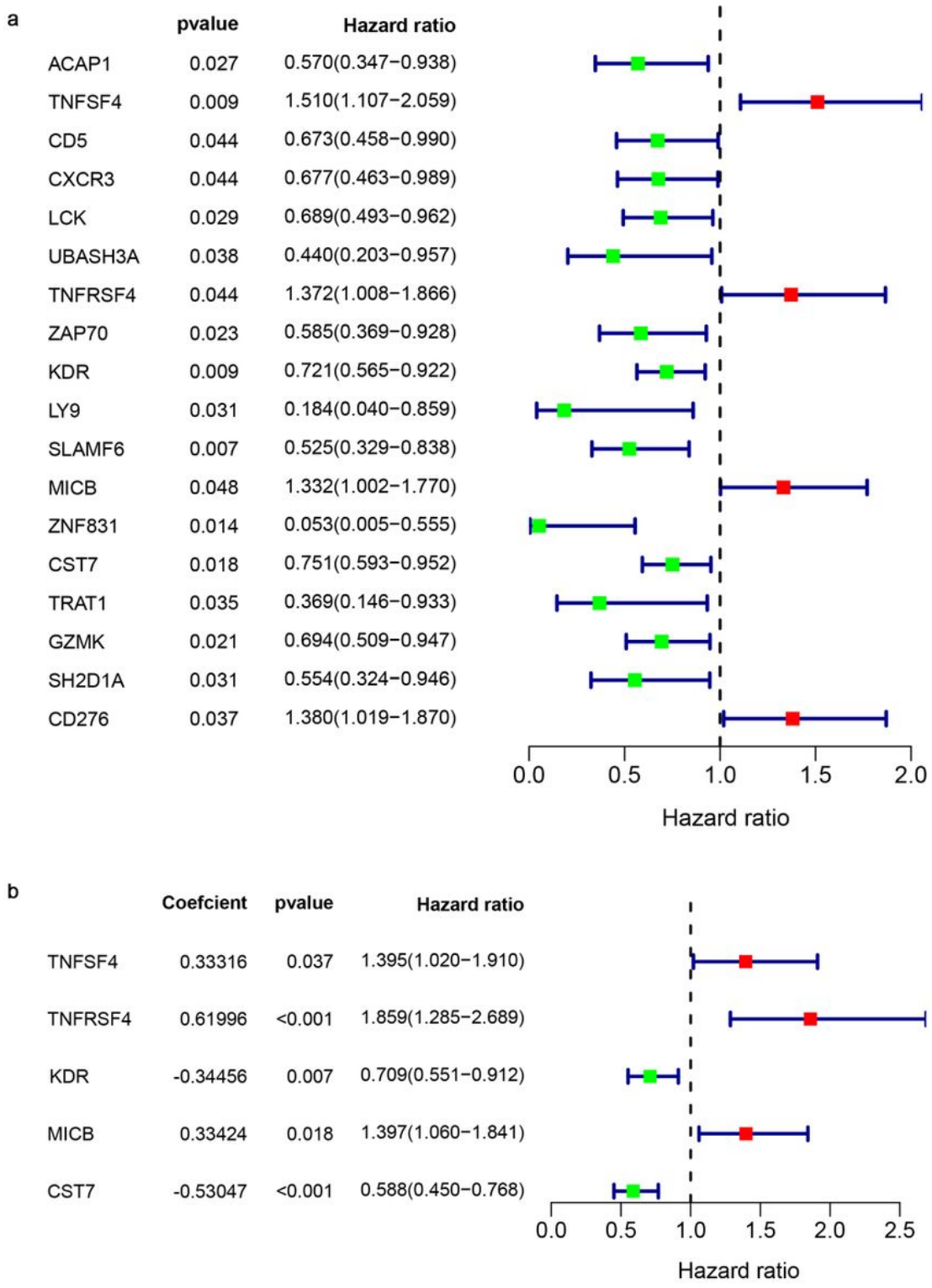

Figure 10

The development of prognostic gene signatures based on 78 ASF1B-associated immunomodulators. (a) Univariate COX regression of 78 ASF1B-associated immunomodulators. (b) The hazard ratios and coefcient of ASF1B-associated prognostic genes of multivariate COX regression.

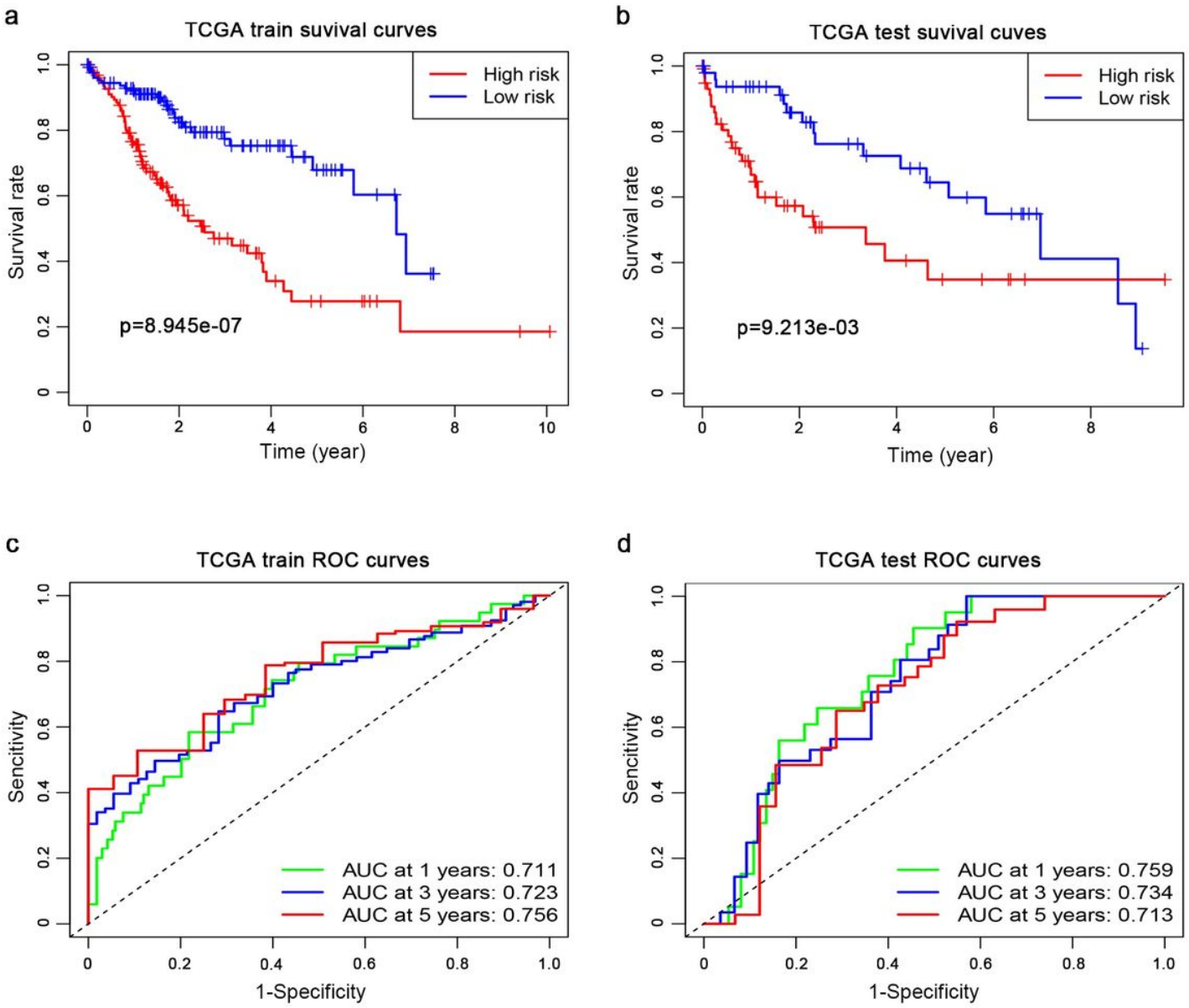

Figure 11

Establishment and internal validation of prognostic model based on risk-score of ASF1B-associated prognostic immunomodulators. (a) Survival curves of the high and low-risk group of the TCGA train set. (b) Survival curves of the high and low-risk group of the TCGA test set. (c) Time-dependent ROC curves of ASF1B-associated prognostic model of the TCGA train set. (d) Time-dependent ROC curves of ASF1B-associated prognostic model of the TCGA test set.

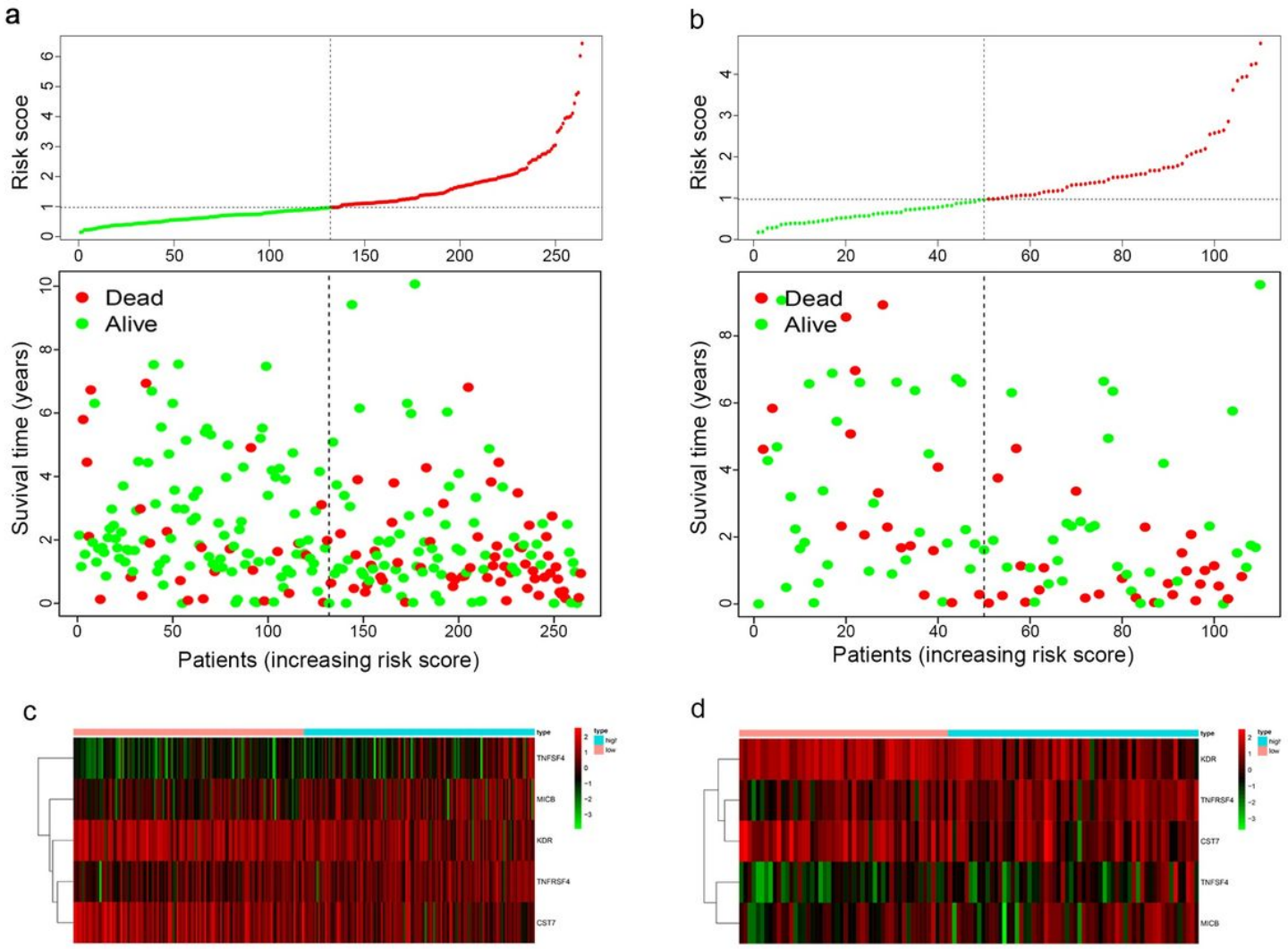

Figure 12

Characteristics of the ASF1B-associated prognostic signature in the TCGA dataset. The dotted line is the optimal cut-of value for dividing HCC patients into high and low-risk groups. (a) The distribution of risk-score and the survival status of HCC patients in train set. (b) The distribution of risk-score and the survival status of HCC patients in test set. (c) Heatmap of the ASF1B-associated prognostic signature expression profiles between the high and low-risk groups in train set. (d) Heatmap of the ASF1B-associated prognostic signature expression profiles between the high and low-risk groups in test set.

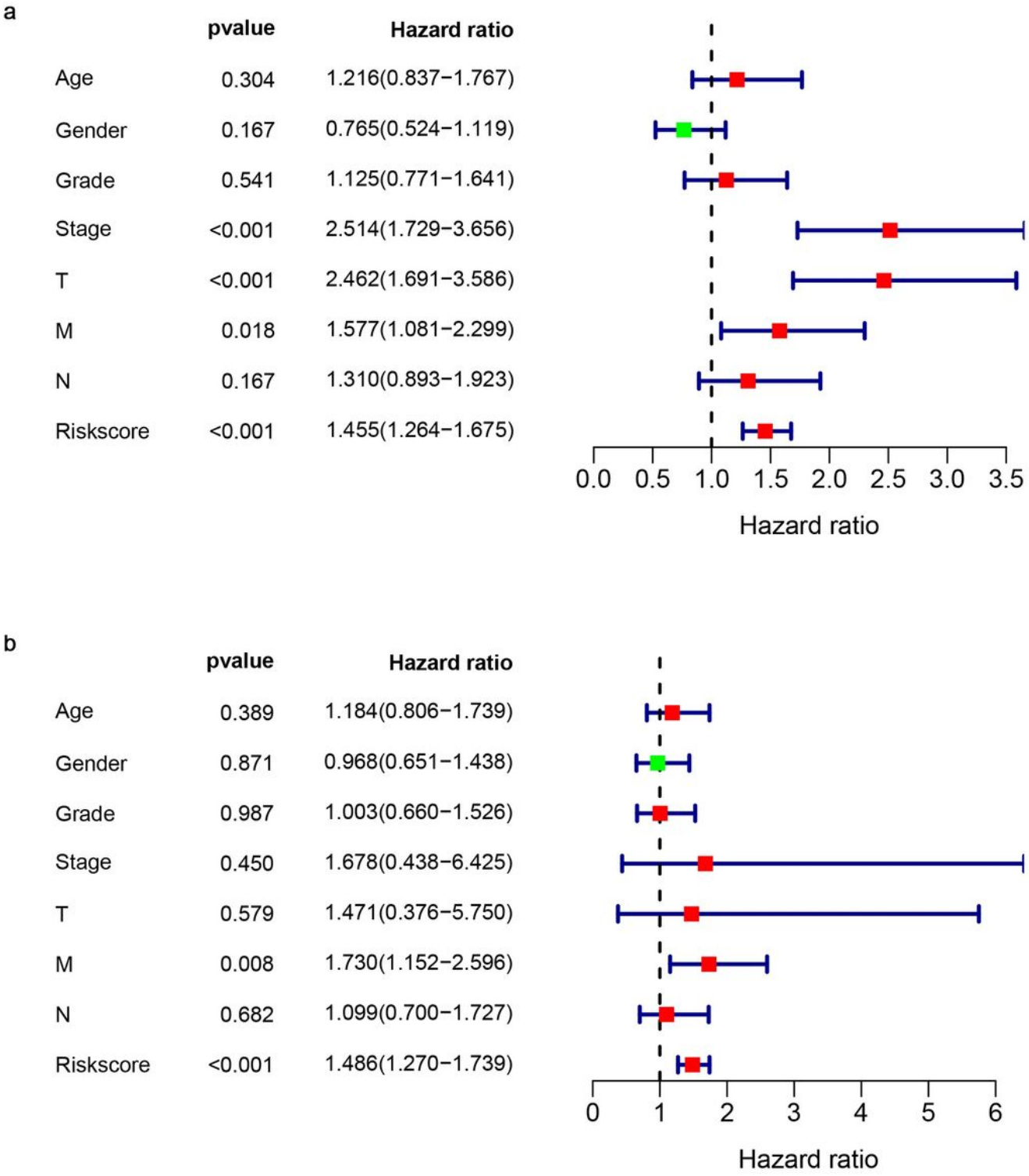

Figure 13

The prognostic value of the ASF1B-associated prognostic signature in the TCGA dataset. (a) Univariate COX analysis of risk-score and clinical characteristics. (b) Multivariate COX analysis of risk-score and clinical characteristics.

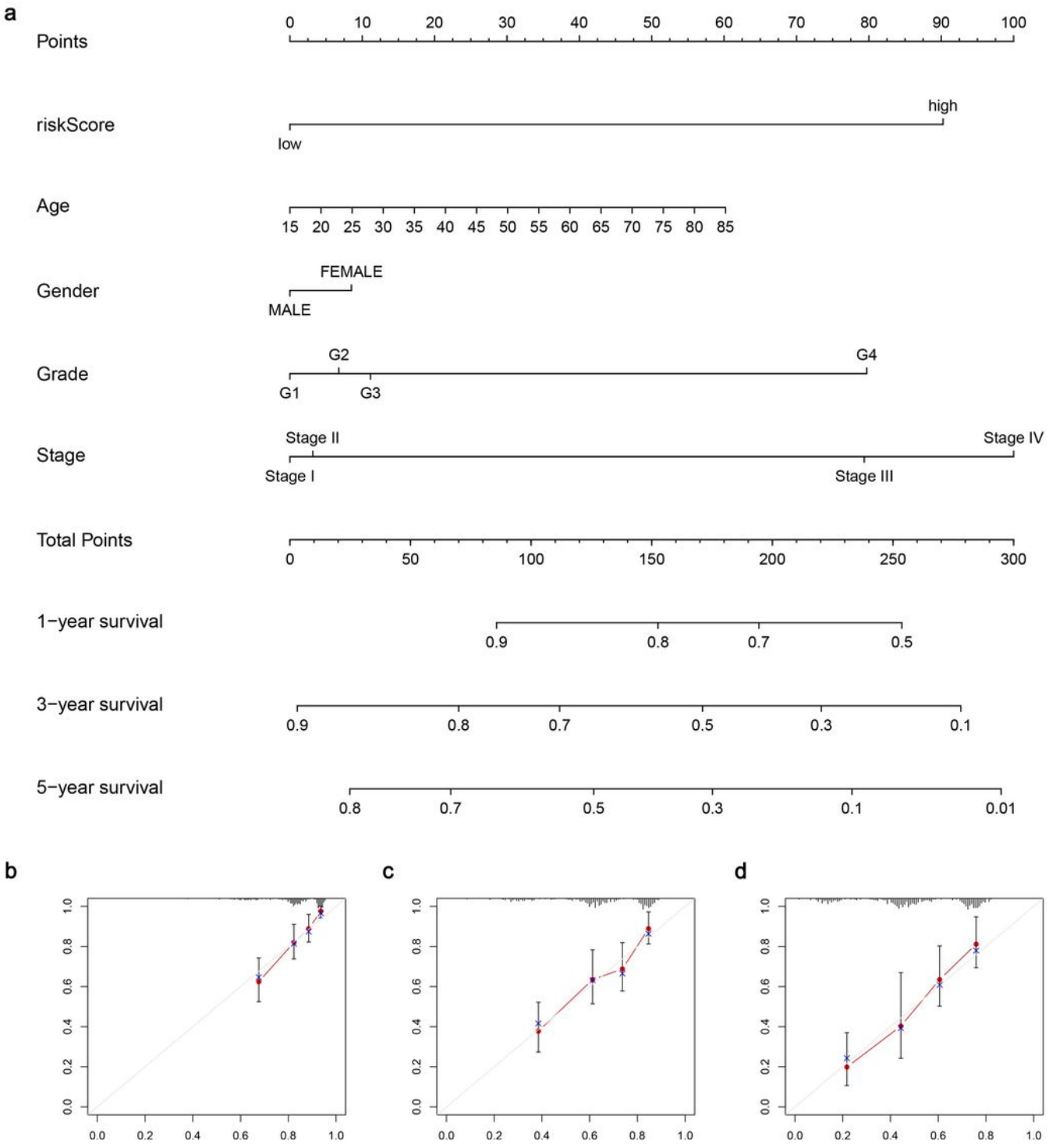

Figure 14

Establishment of the prognostic nomogram with the inclusion of the risk-score. (a) A nomogram for predicting 1- and 3-year survival possibilities of individual HCC patients. The calibration curve of 1-year (b), 3-year (c) and 5-year (d) survival of HCC patients . The dashed line represented a perfect uniformity between nomogram-predicted and real possibilities.

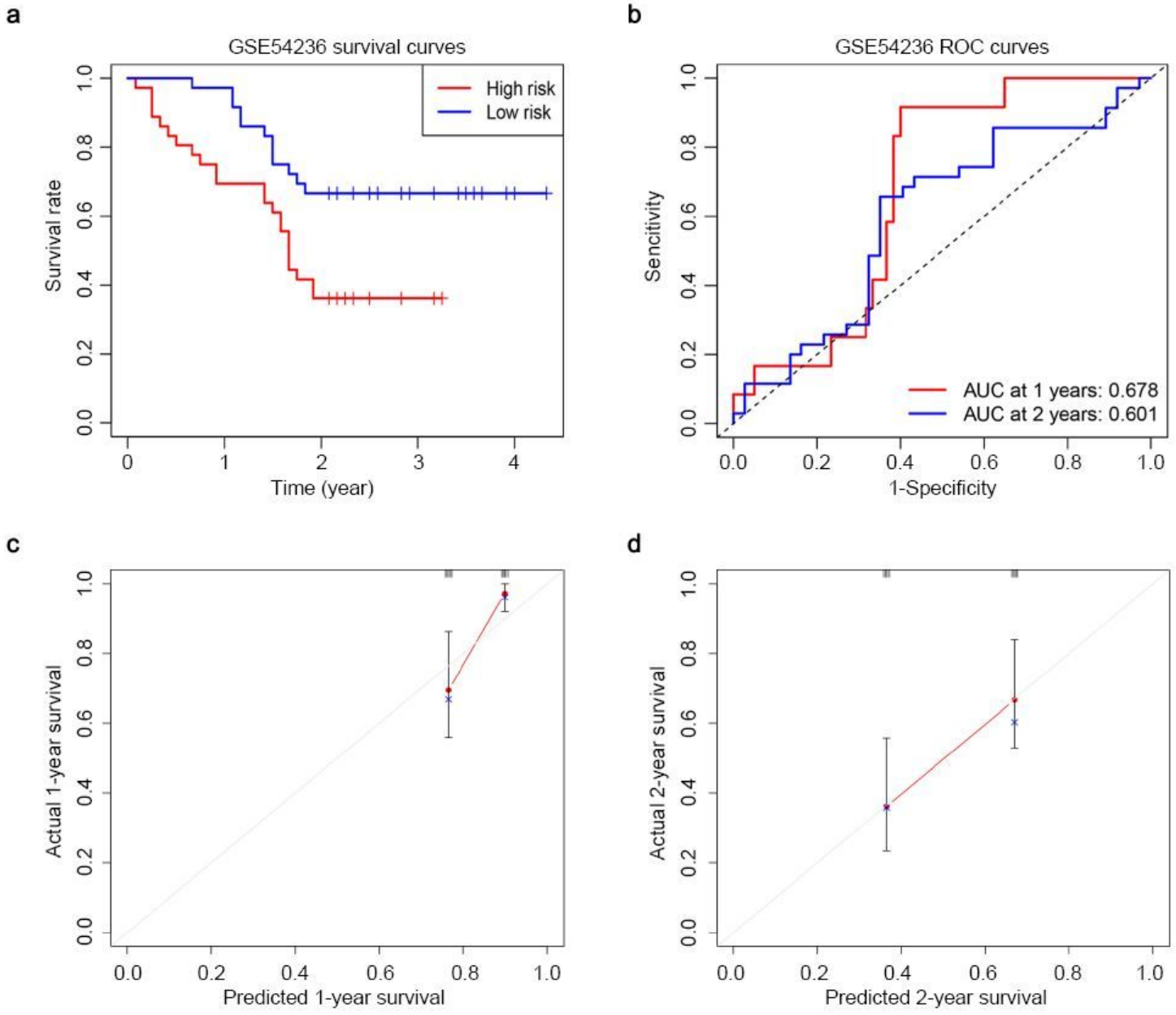

Figure 15

External validation of the ASF1B-associated prognostic risk model. (a) Kaplan-Meier survival curves of HCC patients in the high and low-risk group in GSE54236. (b) Time-dependent ROC curves analysis of the prognostic risk model based on risks core for 1- and 2-year OS probability in GSE54236. Calibration plots of 1-year (c) and 2-year (d) predicted survival.

Supplementary Files

This is a list of supplementary files associated with this preprint. Click to download.

- SupplementaryDataset1.txt
- SupplementaryDataset2.txt

- SupplementaryDataset3.txt
- SupplementayrFigure1.pdf